Table of content

- **S8: Residual analysis of experimental data supports performance improvement of HyU.**
- **S9: Application of denoising filters reveals improved results with lower residuals.**
- **S10: Comparison of residual images for LU and HyU highlights improved HyU performance.**
- **S11: Residual maps facilitate identification of independent spectral components.**
- **S12: HyU analysis of 36 hpf Casper zebrafish demonstrates feasibility of unmixing only intrinsic signals**
- **S13: Speed comparison and improvement plots of multiple unmixing algorithms in their Original form vs HyU encoded.**
- **S14: Residuals in synthetic data and experimental data.**

Tables:

- **S1 data**

Movies:

- **V1: HyU vs LU unmixing results**
- **V2: 3 colors 300 mins time-lapse video**
- **V3: 9 colors time-lapse video with intrinsic and extrinsic signals**

Notes:

- **N1: Identification of spectra and new components with HyU**
- **N2: HyU in autofluorescent data**
- **N3: Reduced computational costs during unmixing**

Materials and Methods

Zebrafish lines.

Adult fish were raised and maintained as described[1] in strict accordance with the recommendations in the Guide for the Care and Use of Laboratory Animals by the University of Southern California, where the protocol was approved by the Institutional Animal Care and Use Committee (IACUC) (Permit Number: 12007 USC). Upon crossing appropriate adult lines, the embryos obtained were raised in Egg Water (60 µg/ml of Instant Ocean and 75 µg/ml of CaSO4 in Milli-Q water) at 28.5°C with addition of 0.003% (w/v) 1-phenyl-2-thiourea (PTU) around 18hpf to reduce pigment formation.

Transgenic Gt(cltca-Citrine)^{ct116a} line is a genetrap of clathrin, heavy polypeptide a, labeling transport vesicles with heightened expression in the vasculature.[2] Tg(kdrl:mCherry) labels the vasculature and was a kind gift from Ching-Ling Lien (Children's Hospital Los Angeles). Tg(fli1:mKO2)^{ct641ca} labels pan endothelial cells in both blood vessels and lymphatics as previously reported.[3] Tg(ubiq:lyn-tdTomato) labels all cell membrane by expression of lyn-tdTomato from the ubiquitin promotoer, while Tg(ubiq:Lifeact-mRuby) labels actin by expression of LifeAct-mRuby fusion from the ubiquitin promoter.

mpv17a9/a9;mitfaw2/w2 (casper) line was purchased from Zebrafish International Resource Center (ZIRC) and csf1rj4e1/j4e1 (panther) line[4] was a kind gift from David Parichy (Univ. Virginia). We crossed casper with panther to produce triple heterozygote mpv17a9/+;mitfaw2/+;csf1rj4e1/+ F1 generation fish, which were subsequently incrossed to produce F2 generation with 27 combinations of mutational state of these genes. Since csf1rj4e1 phenotype was not clear in F2 adult with casper phenotype, we outcrossed these fish with panther fish to determine the zygocity of csf1rj4e1 mutation based on the frequency of larva with xanthophores (heterozygote and homozygote produced 50%- and 0%-fraction of xanthophore-positive larva, respectively) by fluorescence microscopy. The casper;csf1rj4e1/j4e1 line is viable and reproducible; we outcrossed either casper;csf1rj4e1/j4e1 line or casper;csf1rj4e1/+ line with other fluorescent transgenic lines over several generations to obtain fish harboring multiple transgenes on casper background either in the presence or absence of xanthophores.

Sample preparation

Transgenic zebrafish lines were intercrossed over multiple generations to obtain embryos with multiple combinations of the transgenes. All lines were maintained as heterozygous for each transgene. Embryos were screened using a fluorescence stereo microscope (Axio Zoom, Carl Zeiss) for expression patterns of individual fluorescence proteins before imaging experiments. A confocal microscope (LSM 780, Carl Zeiss) was used to isolate Tg(ubiq:Lifeact-mRuby) lines from Tg(ubiq:lyn-tdTomato) lines by distinguishing spatially- and spectrally-overlapping signals.

For *in vivo* imaging, 5–6 zebrafish embryos at 18 to 72 hpf were immobilized and placed into 1% UltraPure low-melting-point agarose (catalog no. 16520-050, Invitrogen) solution prepared in 30% Danieau (17.4 mM NaCl, 210 M KCl, 120 M $MgSO_47H_2O$, 180 M $Ca(NO_3)_2$, 1.5 mM

HEPES buffer in water, pH 7.6) with 0.003% PTU and 0.01% tricaine in an imaging dish with no. 1.5 coverglass bottom, (catalog no. D5040P, WillCo Wells). Following solidification of agarose at room temperature (1–2 min), the imaging dish was filled with 30% Danieau solution and 0.01% tricaine at 28.5 °C.

Image Acquisition.

Images were acquired on a Zeiss LSM 780 laser confocal scanning microscope equipped with a 32-channel detector using 40x/1.1 W LD C-Apochromat Korr UV-VIS-IR lens at 28ºC.

Samples of Gt(cltca-Citrine), Tg(ubiq:lyn-tdTomato), Tg(fli1::mKO2), and Tg(ubiq:Lifeact-mRuby), were simultaneously imaged with 488 nm and 561 nm laser excitation, for citrine, tdTomato, mKO2, and mRuby. A narrow 488 nm/561 nm dichroic mirror was used to separate excitation and fluorescence emission. Samples were imaged with a 2-photon laser at 740 nm to excite autofluorescence, using a 690nm lowpass filter to separate excitation and fluorescence. For all samples, detection was performed at the full available range (410.5-694.9nm) with 8.9nm spectral binning

Supplementary Table 1 provides the detailed description of the imaging parameters used for all images presented in this work.

Hyperspectral Fluorescence Image Simulation

The model simulates spectral fluorescent emission by generating a stochastic distribution of photons with profile equivalent to the pure reference spectra (as described in Sup. Note 1). The effect of photon starvation, commonly observed on microscopes, is synthetically obtained by manually reducing the number of photons in this stochastic distribution. Detection, Poisson and signal transfer noises are then added to produce 32-channel fluorescence emission spectra that closely resemble those acquired on microscopes. The simulations include accurate integration of dichroic mirrors and imaging settings.

Image analysis.

Independent Spectral Signatures

Independent spectral fingerprints for fluorescent signals were obtained by imaging single labelled samples in areas morphologically and physiologically known to express the specific fluorescence. Those fingerprints were compared with literature fingerprints and manually corrected to reduce noise.

For autofluorescent signals, spectrum for Elastin was obtained experimentally and compared with literature. [5] Spectra for Nicotinamide Adenine Dinucleotide (NADH) free, NADH bound, Retinoic acid, Retinol and Flavin Adenine Dinucleotide (FAD) were acquired from in vitro solutions using the microscope. NADH free from B-Nicotinamide Adenine Dinucleotide (Sigma-Aldrich, St. Luis, MO, #43420) in Phosphate Buffered Saline (PBS) solution. NADH bound from B-Nicotinamide Adenine Dinucleotide and L-Lactic Dehydrogenase (Sigma-Aldrich, #43420, #L3916) in PBS. Retinoic acid from a solution of

Retinoic Acid (Sigma-Aldrich, #R2625) in Dimethylsulfoxide (DMSO). Retinol from a solution of Retinol synthetic (Sigma-Aldrich, #R7632) in DMSO. FAD from Flavin Adenine Dinucleotide Disodium Salt Hydrate (Sigma-Aldrich, #F6625) in PBS.

Phasor analysis.

For each pixel in a dataset, the Fourier coefficients of its normalized spectra define the coordinates $(G(n), S(n))$ in the phasor plane, where:

$$G(n) = \frac{\sum_{\lambda_s}^{\lambda_f} I(\lambda)\cos(n\omega\lambda)\Delta\lambda}{\sum_{\lambda_s}^{\lambda_f} I(\lambda)\Delta\lambda} \quad (1)$$

$$S(n) = \frac{\sum_{\lambda_s}^{\lambda_f} I(\lambda)\sin(n\omega\lambda)\Delta\lambda}{\sum_{\lambda_s}^{\lambda_f} I(\lambda)\Delta\lambda} \quad (2)$$

$$\omega = \frac{2\pi}{c} \quad (3)$$

Where λ_s and λ_f are starting and ending wavelengths respectively; I is the measured intensity; c is the number of spectral channels (32 in our case), and n the harmonic number[6]. In this work, we utilized the first harmonic ($n = 1$) for the autofluorescent signals and the second harmonic ($n = 2$) for fluorescent signals based on the sparsity of independent spectral components. A two-dimensional histogram with dimensions (S, G) is applied to the phasor coordinates in order to group pixels with similar spectra within a single square bin. We define this process as phasor encoding.

Linear Unmixing

The hypothesis for linear unmixing in this work is that given *i* independent spectral fingerprints (*fp*), each collected spectrum (*I(λ)*) is a linear combination of *fp*, and the sum of each *fp* contribution (R) is 1.

$$I(\lambda) = W_1R_1fp_1 + W_2R_2fp_2 + \cdots + W_iR_ifp_i + N \quad (4)$$

$$\Sigma R_i = 1 \quad (5)$$

where R_i is the ratio, W_i the weight, and N the noise. The acquired spectra are collected in the original spectral cube with shape (t,z,c,y,x), with t as time, c as channel and x,y,z spatial dimensions.

i spectral vectors, fp_i, need to be provided to the unmixing function. It is assumed that there are identical weights for all fp, and a low value for noise N. Under these conditions, we obtain R_i by applying a Jacobian Matrix Inversion[7]:

$$\begin{bmatrix} \sum_x w(x)\frac{\partial f^0}{\partial \alpha_1}\frac{\partial f^0}{\partial \alpha_1} & \sum_x w(x)\frac{\partial f^0}{\partial \alpha_1}\frac{\partial f^0}{\partial \alpha_2} & \cdots \\ \sum_x w(x)\frac{\partial f^0}{\partial \alpha_2}\frac{\partial f^0}{\partial \alpha_1} & \sum_x w(x)\frac{\partial f^0}{\partial \alpha_2}\frac{\partial f^0}{\partial \alpha_2} & \cdots \\ \vdots & \vdots & \ddots \end{bmatrix} \begin{bmatrix} \alpha_1 - {\alpha_1}^0 \\ \alpha_2 - {\alpha_2}^0 \\ \vdots \end{bmatrix} = \begin{bmatrix} \sum_x w(x)[y(x) - f^0(x)]\frac{\partial f^0}{\partial \alpha_1} \\ \sum_x w(x)[y(x) - f^0(x)]\frac{\partial f^0}{\partial \alpha_1} \\ \sum_x w(x)[y(x) - f^0(x)]\frac{\partial f^0}{\partial \alpha_1} \end{bmatrix} \quad (6)$$

In the pixel-by-pixel linear unmixing implementation in this work, the Jacobian Matrix inversion is applied on the acquired spectrum in each pixel with dimensions (t,z,c,y,x). Resulting ratios for each spectral vector are assembled in the form of a ratio cube with shape (t,z,*i*,y,x) where x,y,z,t are the original image spatial and time dimensions, respectively and *i* is the number of input spectral vectors. The ratio cube (t,z,*i*,y,x) is multiplied with the integral of intensity over channel dimension of the original spectral cube, with shape (t,z,y,x), to obtain the final resulting dataset with shape (t,z,*i*,y,x).

Hybrid Unmixing - Linear Unmixing

In the Hybrid Unmixing implementation, Jacobian Matrix Inversion is applied on the average spectrum of each phasor bin with dimensions (c,s,g) where g and s are the phasor histogram sizes and c is the number of spectral channels acquired. The average spectra in each bin is calculated by using the phasor as an encoding, to reference each original pixel spectra to a bin. Resulting ratios for each component channel are assembled in the form of a phasor bin-ratio cube with shape (*i*,s,g) where i is the number of input independent spectra *fp* (Linear Unmixing section). This phasor bin-ratio cube is then referenced to the original image shape, forming a ratio cube with shape (t,z,*i*,y,x) where x, y, z, t are the original image dimensions. We multiply the ratio cube with the integral of intensity over channel dimension of the original spectral cube, with shape (t,z,y,x), obtaining a final result dataset with shape (t,z,*i*,x,y).

HyU Algorithm

The pseudo-code utilized for the HyU algorithm is as follows:

Input: *I(x,y,c,z,t) [5D hyperspectral image]*
U(i,c) [Reference spectra (n spectra))]

Output: *I_U(x,y,i,z,t) [Multi-channel unmixed image]*

Procedure:

HYU(I(x,y,c,z,t), U(n, c))

// Single Harmonic Fourier Transform

G(x,y,z,t), S(x,y,z,t) = phasor_transform(I(x,y,c,z,t))

// 2D Histogram of G and S values

H(g,s) = histogram2d(G(x,y,z,t) S(x,y,z,t))

// Averaging of hyperspectral image over phasor histogram

I_H(g,s,c) = phasor_average(I(x,y,c,z,t), H(g,s))

// Linear Unmixing of averaged hyperspectral image

I_U(g,s,i) = LU(I_H(g,s,c), U(i,c))

// Reference unmixed phasor image back to original image dimensions

I_U(x,y,i,z,t) = reverse_phasor_reference(I_U(g,s,i)

return I_U(x,y,i,z,t)

Other unmixing algorithms

Unmixing algorithms utilized for speed comparisons with the HyU algorithm (Supplementary Figure 13) were plugged in the unmixing step of the analysis pipeline and sourced as follows. Non-negative Constrained Least Squares and Fully Constrained Least Squares from pysptools.abundance_maps (https://pysptools.sourceforge.io/abundance_maps.html). Robust Non-Negative Matrix Factorization[8] python implementation was obtained from (https://github.com/neel-dey/robust-nmf)

Data Visualization

Rendering of final result datasets were performed using Imaris 9.5-9.7. In Figures 2 and 3, contrast settings (minimum, maximum, gamma) for each channel were set to be equal to provide reasonable comparison between HyU and LU results. Gamma was set to 1, no minimum threshold was applied, and the maximum for each channel was set to 1/3 of the maximum intensity. The images were rendered using Maximum Intensity Projection (MIP), and for improving display, they were digitally resampled in the z-direction, maintaining a fixed xy ratio to attenuate the gap generated from sparse sampling z-wise on the microscope.

Timelapse registration

A customized python script (Supplementary Code) was first utilized to pad the number of z slices across multiple time points, obtaining equally sized volumes. The "Correct 3D drift" plugin[9] (https://imagej.net/Correct_3D_Drift) in FIJI[10] (https://imagej.net/Fiji) was used to register the data.

Code availability

All the relevant code is available from the corresponding author upon reasonable request. Software and instructions can be downloaded from http://bioimaging.usc.edu/software.html#HySP.

Data availability

All the relevant data are available from the corresponding author upon reasonable request. Datasets for Figs.1–6 and simulations are available for download at http://bioimaging.usc.edu/software.html#sampledatasets in the samples section.

Performance quantification

Mean Square Error

For synthetic data, a ground truth is available for comparison of unmixing fidelity between HyU and LU. *fp* contributions, or ratios, were used for quantification, owing to the arbitrary nature of intensity values in microscopy data. We utilize Mean Square Error (MSE) for determining the quality of the ratios in synthetic data. We define *MSE* as the square difference of the ratio recovered by an unmixing algorithm ($r_{unmixed}$) and the ground truth ratio (r) divided by the total number of pixels (n).

$$MSE = \frac{1}{n} |r_{unmixed} - r|^2 \quad (7)$$

To simplify comparison between different unmixing algorithms, we define Relative Mean Square Error (*RMSE*) as:

$$RMSE = \left(\frac{MSE_{LU}}{MSE_{HyU}} - 1\right) * 100\% \quad (8)$$

RMSE measures the improvement in *MSE* when using HyU as compared to LU.

Residuals

For experimental data, in the absence of ground truth, we quantify the performance of the results returned by the unmixing algorithms with the following measurements: Average Relative Residual, Residual Image Map, Residual Phasor Map, and finally, Residual Intensity Histogram.

Residual (R) is calculated as:

$$\text{For image: } R(x, y, c, z, t) = I_{Raw\ Image}(x, y, c, z, t) - I_{Unmixed\ Image}(x, y, c, z, t) \quad (9)$$

$$\text{For phasor: } R(g, s, c) = I_{Raw\ Image}(g, s, c) - I_{Unmixed\ Image}(g, s, c) \quad (10)$$

The spectral intensity difference between the unmixed image and original image for each pixel or phasor bin depend on the following descriptions of the intensity image (I), where:

$$I_{Raw\ Image} = \sum_i r * fp_i + N \quad (11)$$

$$I_{Unmixed\ Image} = \sum_i r_{unmixed} * fp_i \quad (12)$$

The original spectrum ($I_{Raw\ Image}$) is the combination of each independent spectral component (fp) with its ratio (r) plus noise (N). The recovered spectrum is obtained by the multiplication of recovered ratios ($r_{unmixed}$) with each corresponding individual component.

Relative Residual (RR) is calculated as the sum of the residual values over C channels and normalized to the sum of the original intensity values over C channels (with C = 32 in our instrument).

$$RR(x,y,z,t) = \frac{\sum_{c=1}^{C} R(x,y,c,z,t)}{\sum_{c=1}^{C} I_{Raw\ Image}(x,y,c,z,t)} \quad (13)$$

$$RR(g,s) = \frac{\sum_{c=1}^{C} R(g,s,c)}{\sum_{c=1}^{C} I_{Raw\ Image}(g.s.c)} \quad (14)$$

The Average Relative Residual (Supplementary Figure 5) provides a single comparison value for evaluating the performance of different processing methods on the same data, such as the application of multiple filters, applying of various threshold values, and variations in the number of components estimated. Average Relative Residual (RR_{avg}) is defined as the average of the relative residual for every pixel in the image or every phasor bin in the phasor histogram.

$$\text{For image: } RR_{avg} = \frac{\sum_t \sum_z \sum_y \sum_x RR}{xyzt} \quad (15)$$

$$\text{For Phasor: } RR_{avg} = \frac{\sum_s \sum_g RR}{gs} \quad (16)$$

The Residual Image Map visualizes the residual values for each pixel of the image (Supplementary Figure 4). Regions with higher residual values appear to characterize portions of the dataset with increased amount of noise or where an unexpected spectral signature is present.

Residual Image Maps ($R_{img\ map}(x,y)$) project the Relative Residual (RR) cube to the 2D image shape for each voxel, providing an estimated visualization of an algorithm ratio recovery performance in the spatial context of the original image.

$$R_{img\ map}(x,y) = \sum_{z,t} RR(x,y,z,t) * 100 \quad (17)$$

Residual Phasor Map visualizes residuals for each bin of the phasor histogram (Supplementary Figure 4). These maps allow for insights on where HyU unmixing results have reduced performance in phasor domain and indicate phasor locations of unexpected additional spectral components (Supplementary Figure 5).

$$R_{ph\ map}(g,s) = RR(g,s) * 100 \quad (18)$$

The Residual Intensity Histogram $R_{Int\ Hist}(p,rr)$ (Figure 3 g,h, Supplementary Figure 4d) calculates the distribution of the relative residual in relation to intensity overall all pixels or all phasor bins. Higher residuals appear to be present in regions with lower signal intensity and SNR, providing degraded performance.

For image:

$$R_{Int\ Hist}(p,rr) = count\big(P(x,y,z,t), RR(x,y,z,t)\big)_{p,rr} \quad (19)$$

For phasor:

$$R_{Int\ Hist}(p,rr) = count\big(P(g,s), RR(g,s)\big)_{p,rr} \quad (20)$$

$$P = \frac{\sum_{c=1}^{C} I_{Raw\ Image}}{4*sf} \quad (21)$$

Where p is a bin of the histogram P, rr is a bin of RR, and sf is the factor which converts the number of photons to digital intensity levels.

Image Contrast

Image contrast measures the distinguishability of a detail against the background. Here we use percent contrast to refer the relationship between the highest and lowest intensity in the image.

$$Contrast = \frac{I_S - I_B}{I_B}$$

Where the Intensity of signal average (I_S) is the average of top 20% intensities in the image. The Intensity of background average (I_B), the average of bottom 20% image intensities.

Supplementary Materials:

Supplementary Figure 1

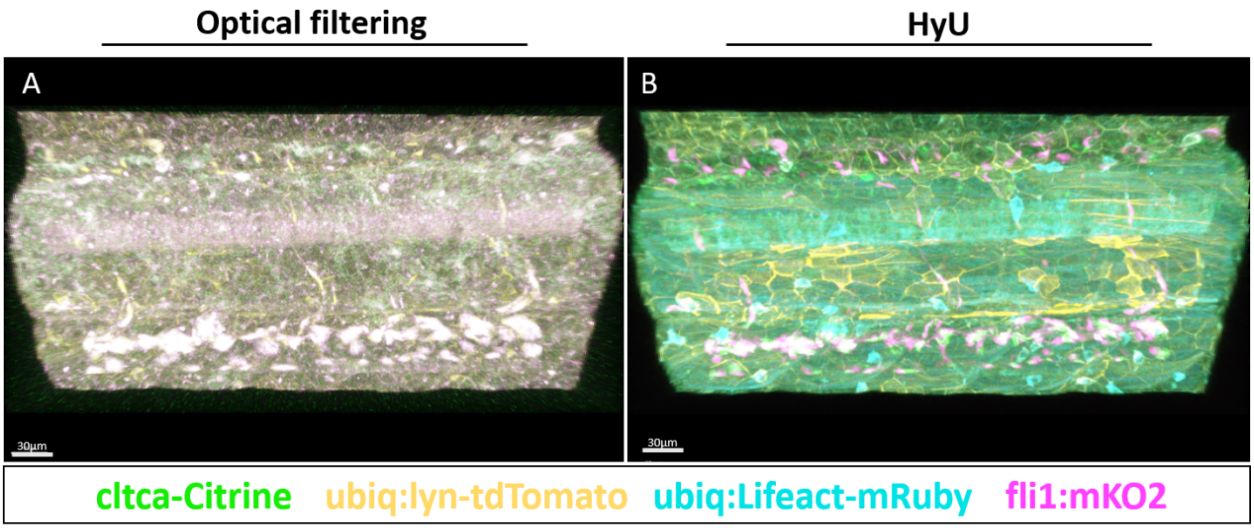

Supplementary Figure 1. HyU unmixing reduces noise and signal bleedthrough compared to traditional bandpass filter imaging. Imaging of a quadra-transgene zebrafish Gt(cltca-citrine);Tg(ubiq:lyn-tdTomato;ubiq:Lifeact-mRuby;fli1:mKO2) (same data as fig. 3) performed with **(A)** 4-channel optical filter imaging and **(B)** multispectral imaging and Hybrid Unmixing (HyU) analysis. Bleed-through from the fluorophores' overlapping emission spectra is present in **A**. This artifact is the result of the sharp spectral discretization imposed on the fluorescent signals by the optical filters, which fail to produce a clean distinction between Citrine (480nm-690nm), mKO2 (525nm-690nm), tdTomato (530nm-690nm) and mRuby (560nm-690nm). Fluorophores are well separated in **B**. Colors in both **A** and **B** represent Citrine (green), mKO2 (yellow), tdTomato (magenta) and mRuby (cyan)

Supplementary Figure 2

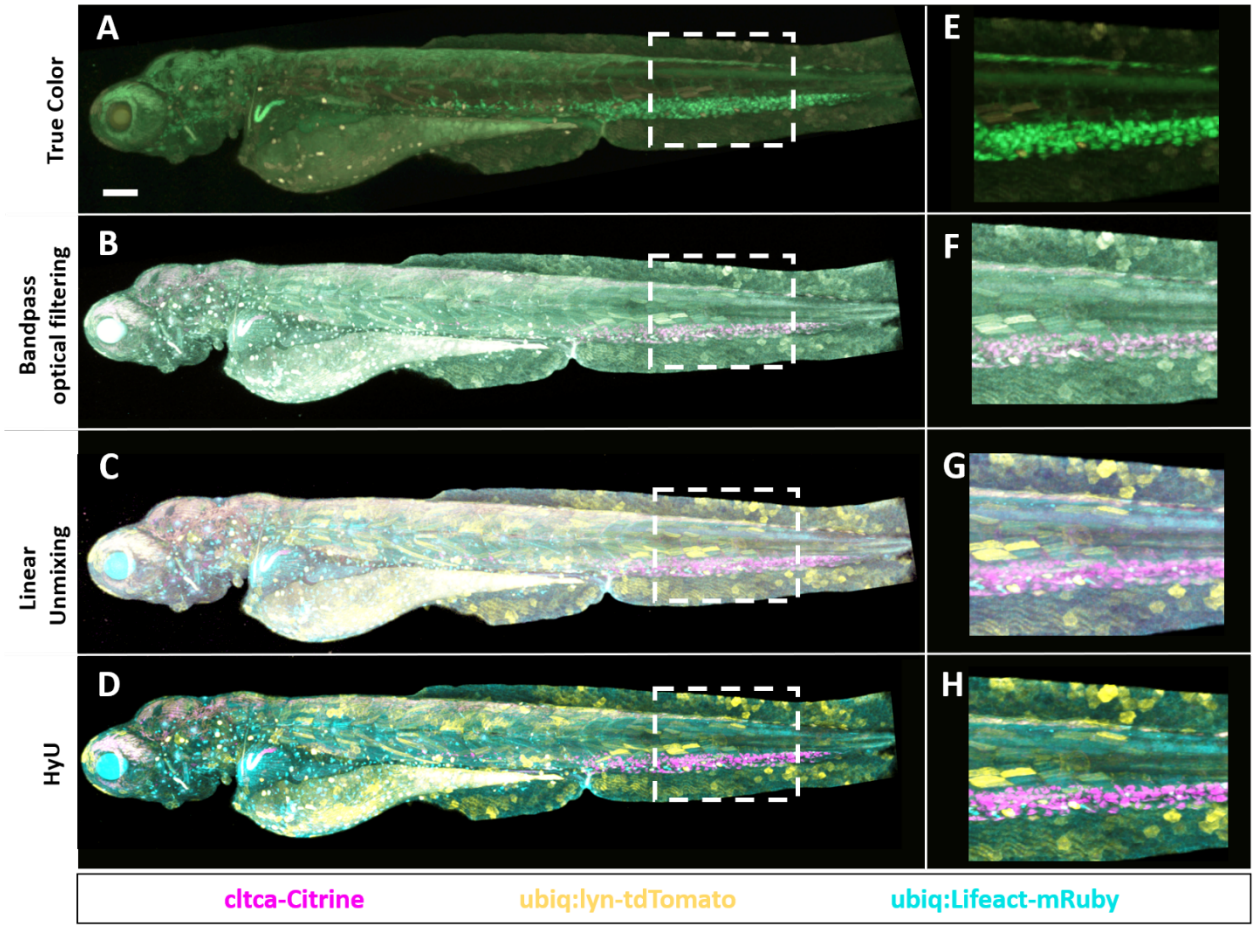

Supplementary Figure 2. **HyU algorithm outperforms current methods. (A)** True-color rendering of a 32 channel tetra-label Gt(cltca-citrine);Tg(ubiq:lyn-tdTomato; ubiq:Lifeact-mRuby) zebrafish shows indistinguishability of multi-label in the absence of analysis. **(B)** Optical filter imaging presents strong bleedthrough across the 4 channels. **(C)** Traditional unmixing provides contrast increase across labels while still affected by incorrect re-assignment of signals. **(D)** Hybrid Unmixing enhances separation of spectral and spatial overlapping signals. **(E-H)** are the zoom in from white boxes in **A**, **B**, **C**, **D** respectively. Scale bar is 100 μm.

Supplementary Figure 3

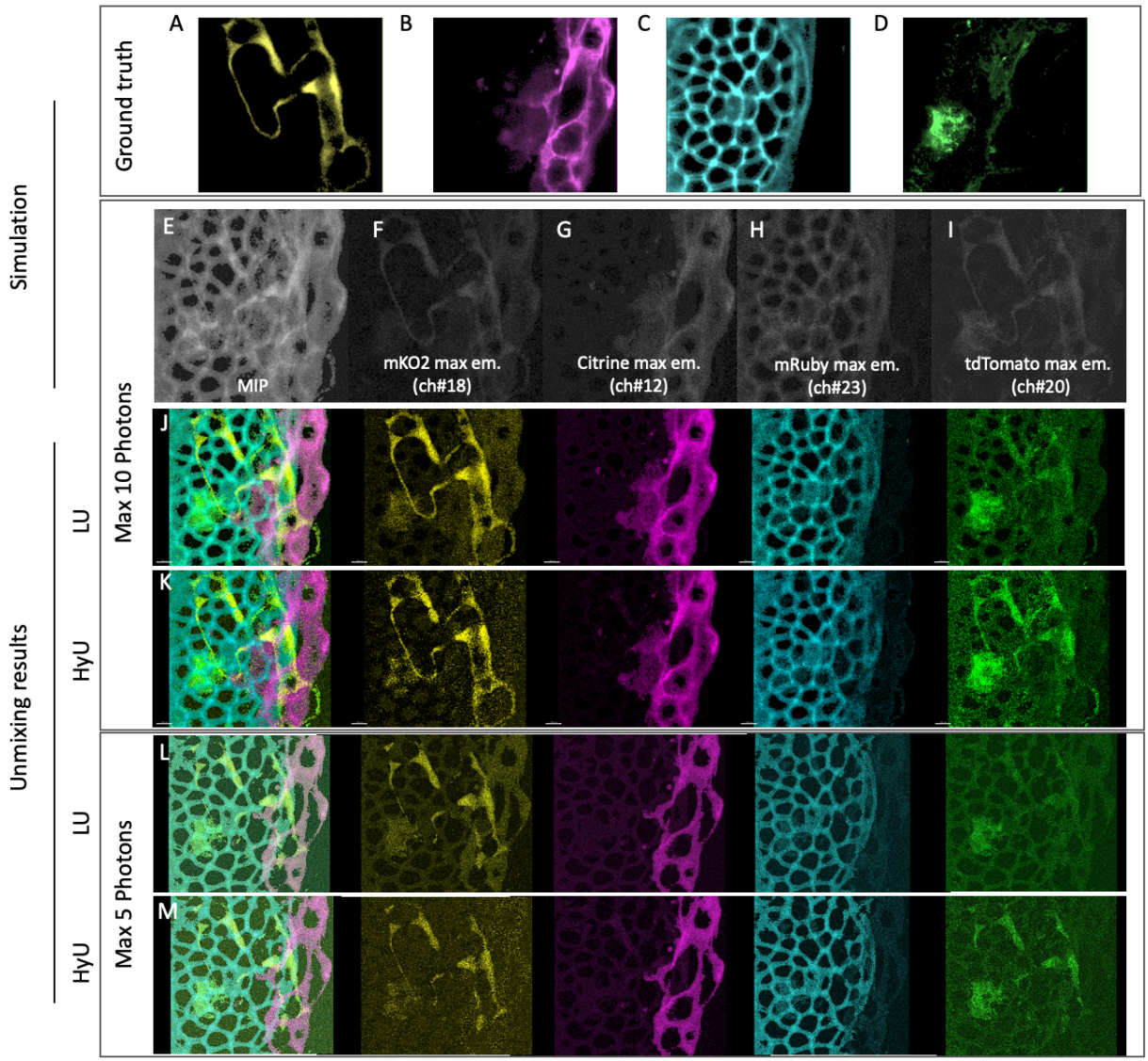

Supplementary Figure 3. Comparison of unmixing results for synthetic data at different SNR demonstrate improved HyU performance. Ground truth photon mask of the four independent fluorescent signals, **(A)** mKO2, **(B)** Citrine, **(C)** mRuby, and **(D)** tdTomato for synthetic data. **(E)** The maximum intensity projection (MIP) of the simulated 32 channel hyperspectral image generated from the four ground truth masks at low signal-to-noise ratio (SNR). In this case, a maximum of 10 photons are simulated for each fluorescent component. (**F**-**I**) Grayscale representation of the maximum emission channel of each component, based on the respective spectra. Unmixing result of **(J)** LU and **(K)** HyU for simulations with a maximum of 10, report decreased performance. In the ultra-low SNR simulation (5 photon at most for each component), both LU **(I)** and HyU **(M)** results are deteriorated, however HyU maintains a 1.5x lower average MSE compared to LU.

Supplementary Figure 4

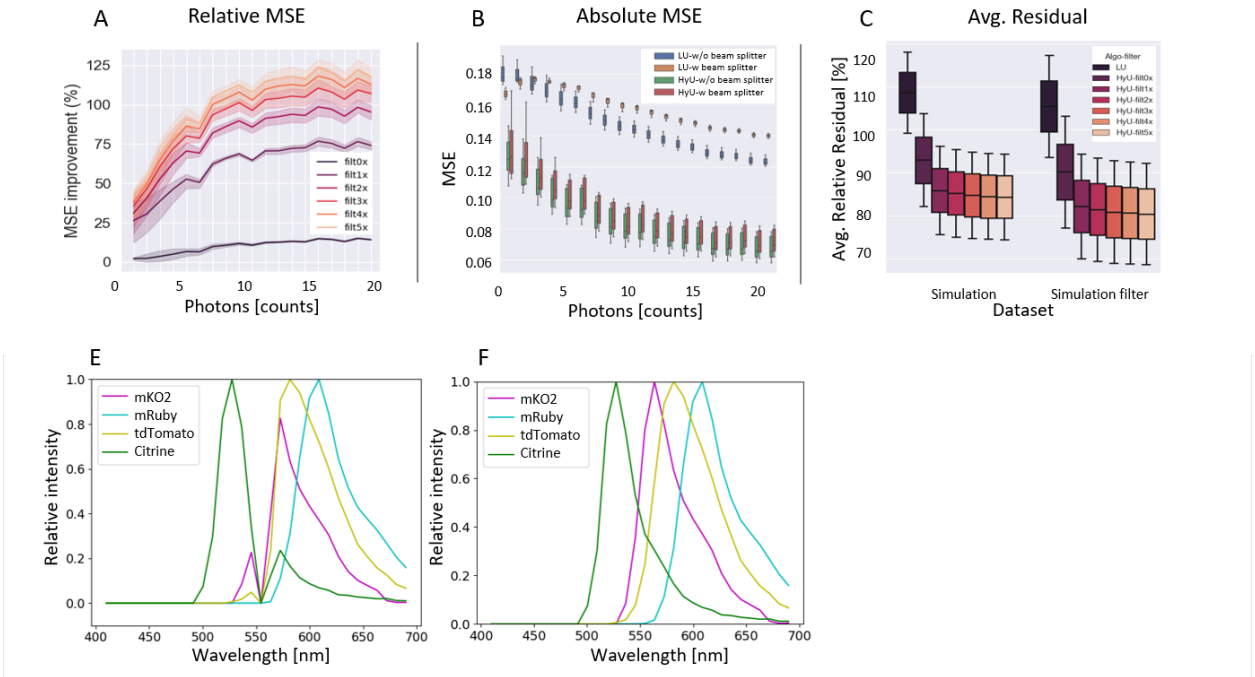

Supplementary Figure 4. Quantification of HyU vs LU unmixing results for synthetic data highlight increased HyU performance. HyU performance is evaluated under several algorithmic parameters and experimental conditions. **(A)** Relative MSE between HyU and LU was calculated as a function of max input photons/spectrum over 5 denoising filters for HyU. The improvement increases both with the number of photons and the number of denoising filters, showing significant differences above 7 photons/spectra with peak at 124%. (**B**) Absolute MSE from LU and HyU algorithms for the same synthetic dataset with and without beam splitters. The addition of optical filters causes the MSE of LU to increase on average by 8% , compared to an average increase of 5% for HyU. (**C**) Average relative residual of synthetic data with and without beam splitters with increasing level of denoising. The average relative residual without beam splitters with denoising (HyU-filt1x – HyU-filt5x) is 83%, compared to 109% for LU. In the absence of denoising filters (filt0x) the average relative residual is 92.9%. Beam splitters were applied in this simulation and both Mean Squared Error (MSE) and residual values were calculated with and without beam splitters. **(E)** Simulated spectral with beam splitter and **(F)** simulated spectral without beam splitter are shown.

Supplementary Figure 5

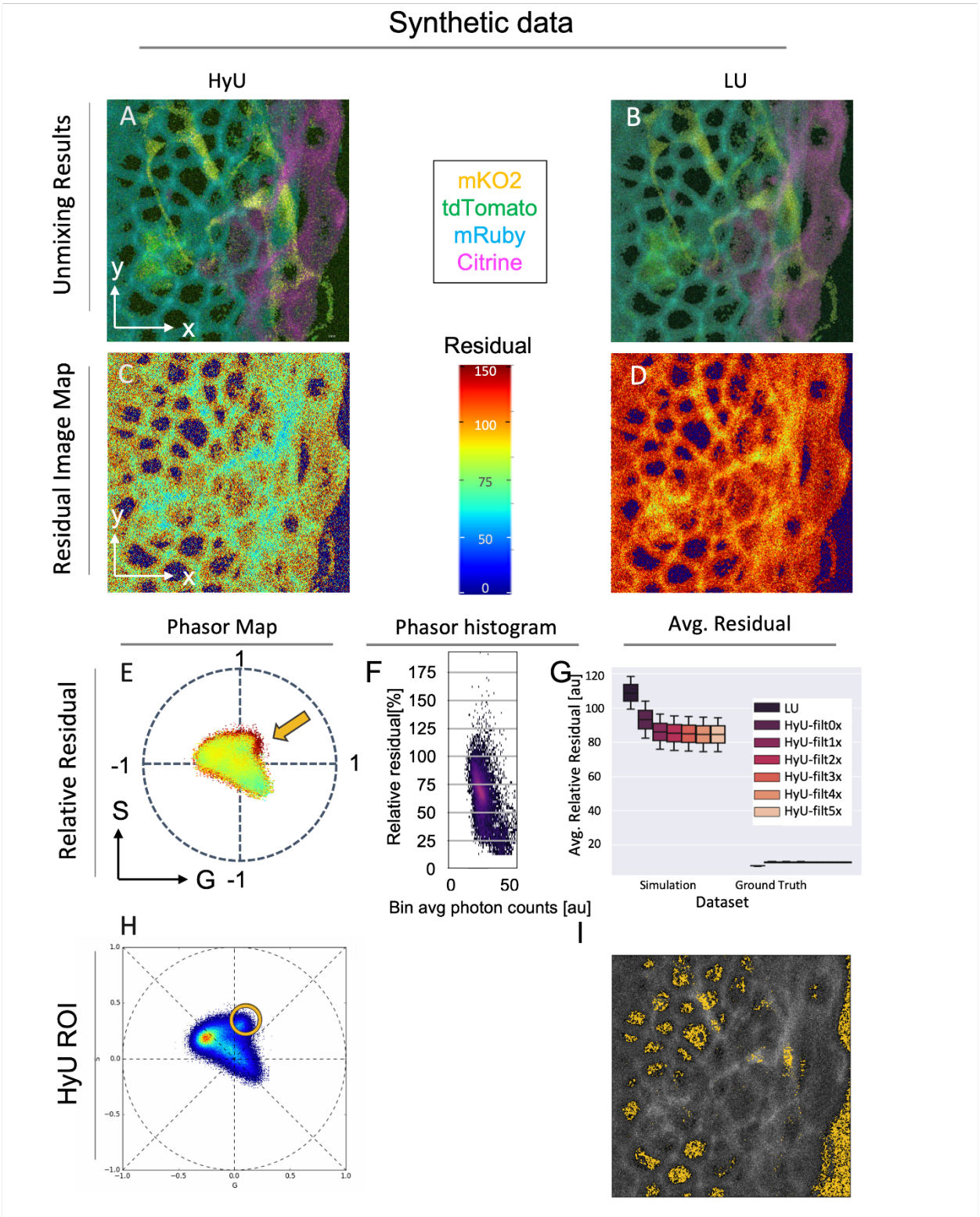

Supplementary Figure 5. Residual analysis for synthetic data identifies locations with reduced algorithm performance. Simulated data in Figure 2 for four fluorescent labels (Citrine, mKO2, tdTomato, mRuby) is analyzed with LU and HyU. Unmixing results for **(A)** HyU and **(B)LU**. Residual Image Map for (**C**) HyU and (**D**) LU results presents regions with higher residual (red) along the boundary between the sample's labelled features and the background, where signal-to-noise drops. The average residual values for LU (118%) are higher than HyU (94%). (**E**) Residual Phasor Map shows higher residual for the background region (arrow), consistently with the results in **C**, **D**. The Jet colorbar scale corresponds to **C**, **D** and **E**. (**F**) Phasor Residual Intensity Histogram maps the average photon counts in each histogram bin in **E** between 0 and 50 photons and presents a trend of decreasing relative residuals with photon number. The (**G**) Average Relative Residual plot shows higher values for LU compared to HyU with different denoising filters applied. Ground truth values are also included for comparison. An **(H)** original phasor plot with 0 threshold and 5 denoising filters applied is presented. The ROI (yellow circle) highlights the background pixels in yellow in the **(I)** average spectral intensity image. The noise from background and residual can be decreased considerably with an intensity threshold.

Supplementary Figure 6

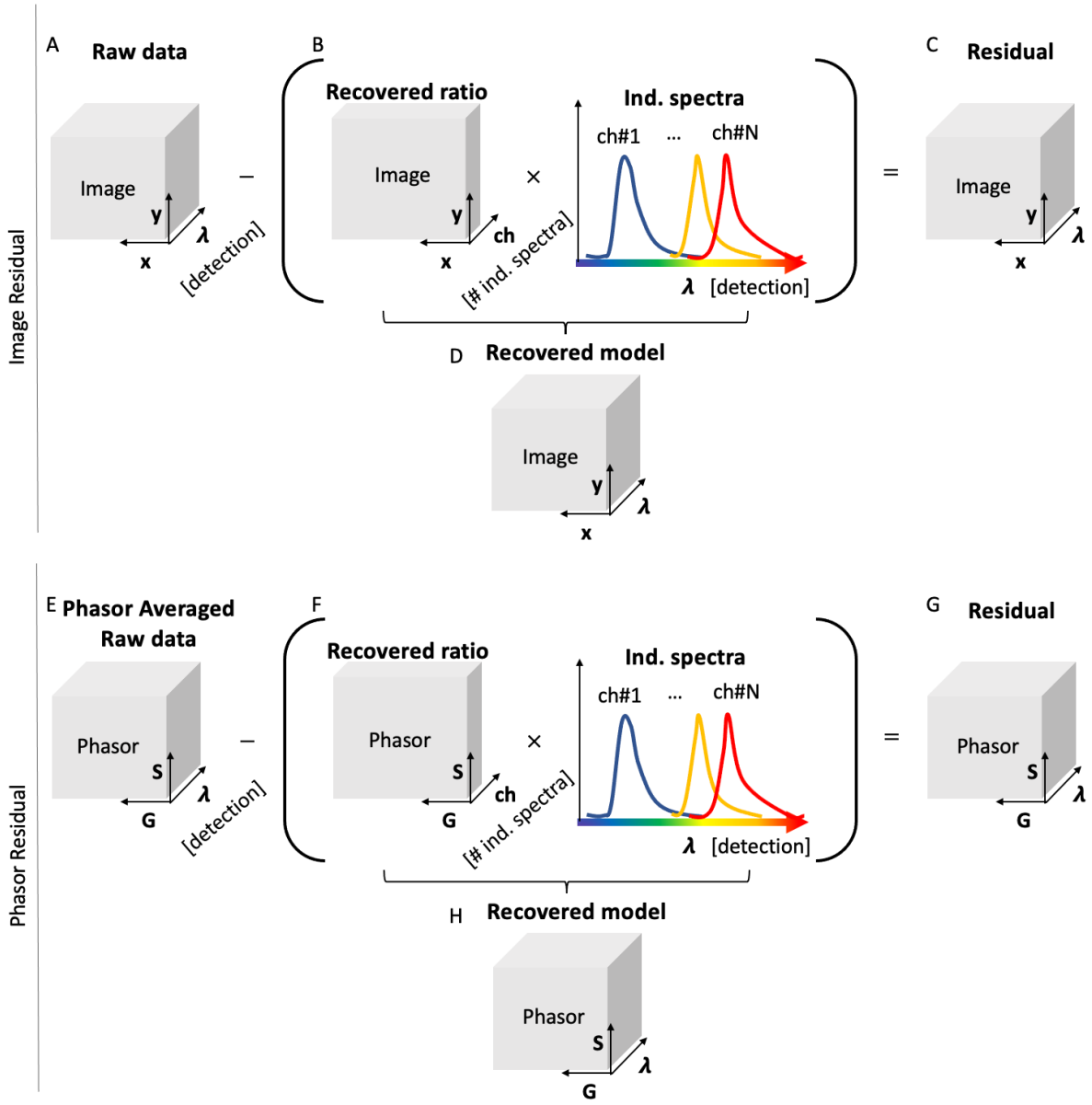

Supplementary Figure 6. **Schematic overview of residual calculation.** Image residual is the residual for image (x, y). **(A)** Raw hyperspectral data cube in dimension of (x, y, λ). x, y is the spatial dimension. λ is the wavelength range from the spectral channel on the detector. **(D)** Recovered model in dimension of (x, y, λ) comes from **(B)** the product of Recover ratio (x, y, ch) and Independent spectra (ch, λ). ch is the number of independent spectra or unmixing component. **(C)** Residual is the difference of Recovered model and Raw data. Same logic for Phasor residual, but instead of (x, y) the dimension of Phasor is composed from the real and imaginary Fourier components (G, S).

Supplementary Figure 7

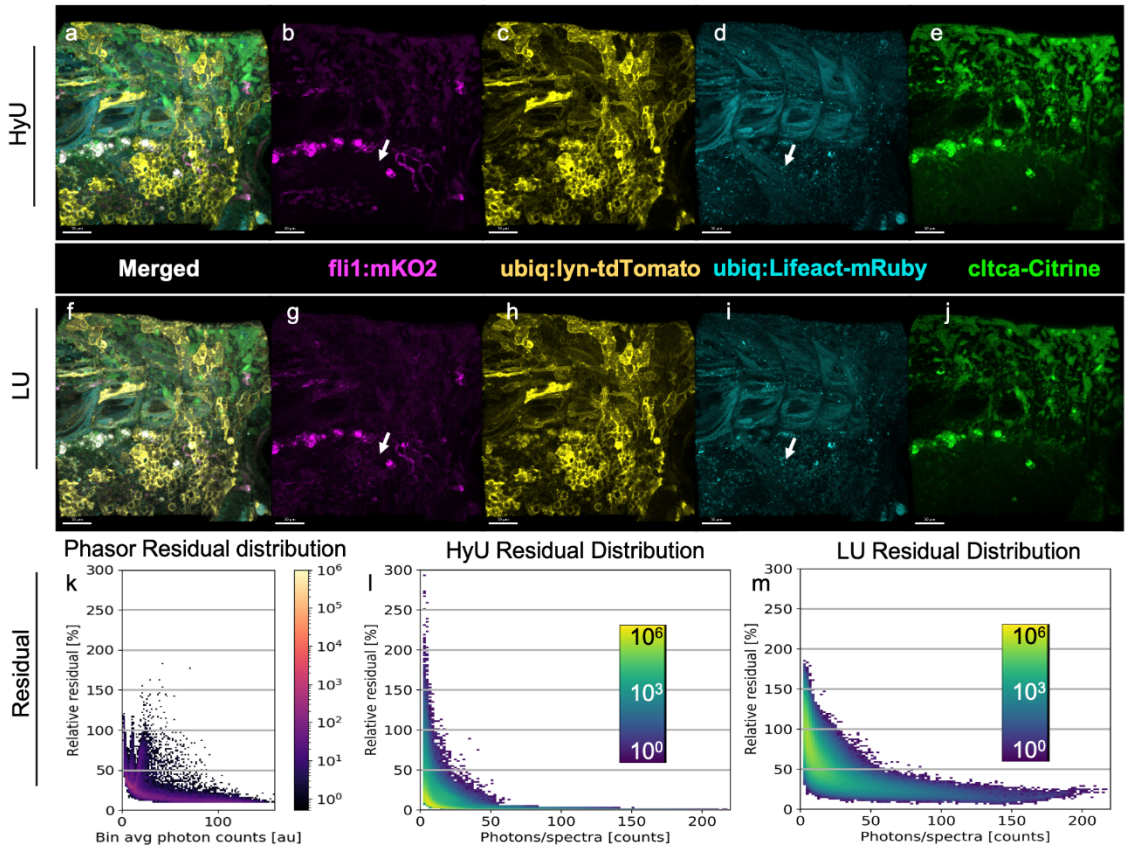

Supplementary Figure 7. Unmixing of a quadra-transgenic zebrafish with HyU and LU highlights improvements in contrast and spatial features. Volumetric zoom-in view of the somites within the trunk region of a 10-dpf Gt(cltca-citrine);Tg(ubiq:lyn-tdTomato; ubiq:Lifeact-mRuby;fli1:mKO2) zebrafish merging all channels in **(A)** HyU and **(B)** LU. (**A-E**) HyU presents a wide dynamic range of intensities with average contrast 1.11-fold higher than LU compared to (**F-J**) LU. In LU, bleed-through from the **(H)** membrane label (arrow) is observed in the **(G)** lymphatic vasculature channel (arrow) and the **(I)** actin channel (arrow). This incorrect re-assignment of intensities is not present in the corresponding HyU channels for **(B)** vasculature and **(D)** actin, where fibers (arrow) are cleanly unmixed. **(K)** Phasor Residual Distribution shows the distribution of relative residual (%) and photon counts in phasor histogram bins. Residual distribution shows the distribution of relative residual (%) and photon counts in histogram pixels for both **(L)** HyU and **(M)** LU.

Supplementary Figure 8

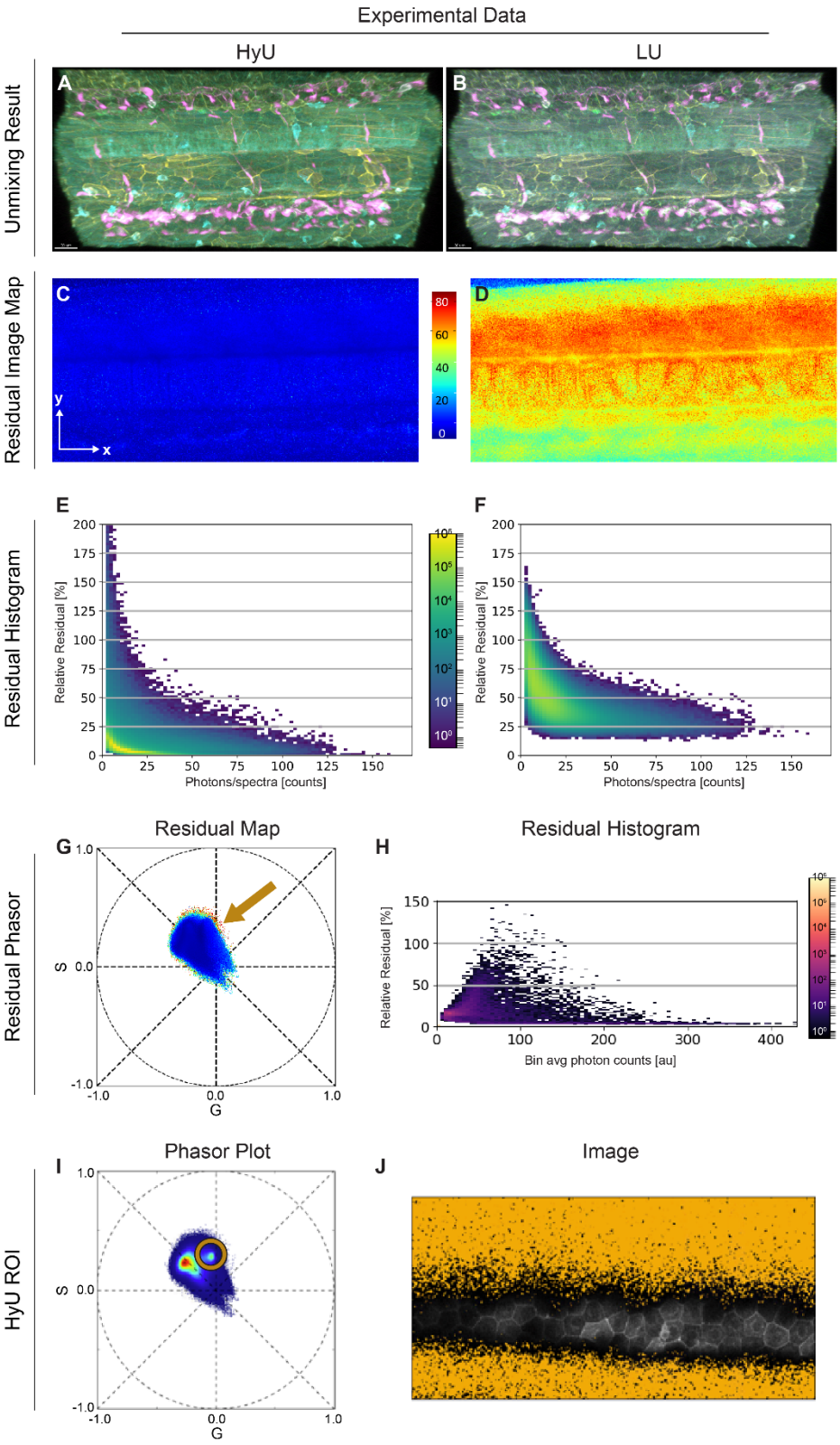

Supplementary Figure 8. Residual analysis of experimental data supports performance improvement of HyU. Residual analysis for multispectral fluorescent data of a 5dpf quadra-transgenic zebrafish Gt((cltca-citrine);Tg (ubq:lyn-tdTomato);(ubiq:Lifeact-mRuby);(fli1:mKO2)) in Figure 3. Unmixing results for **(A)** HyU and **(B)** LU, respectively. Residual Image map of the z-averaged dataset for **(C)** HyU and **(D)** LU show lower residual values for HyU, suggesting improved quality of unmixing. **(E)** Residual distribution relative to the original intensity in each pixel as a function of estimated photon counts per spectrum for LU and (**F**) HyU. **(G)** Residual Phasor Map presents increased residual values in the background region (arrow). Jet colormap scale refers to **C**, **D** and **G**. **(H)** Residual Phasor Histogram for HyU shows distribution of residuals in the broad dynamic range of photons for experimental data. **(I)** Raw phasor with 0 threshold applied and 5 denoising filters, the ROI (yellow circle) highlights the background pixels in the **(J)** average spectral image (showing the first z slice).

Supplementary Figure 9

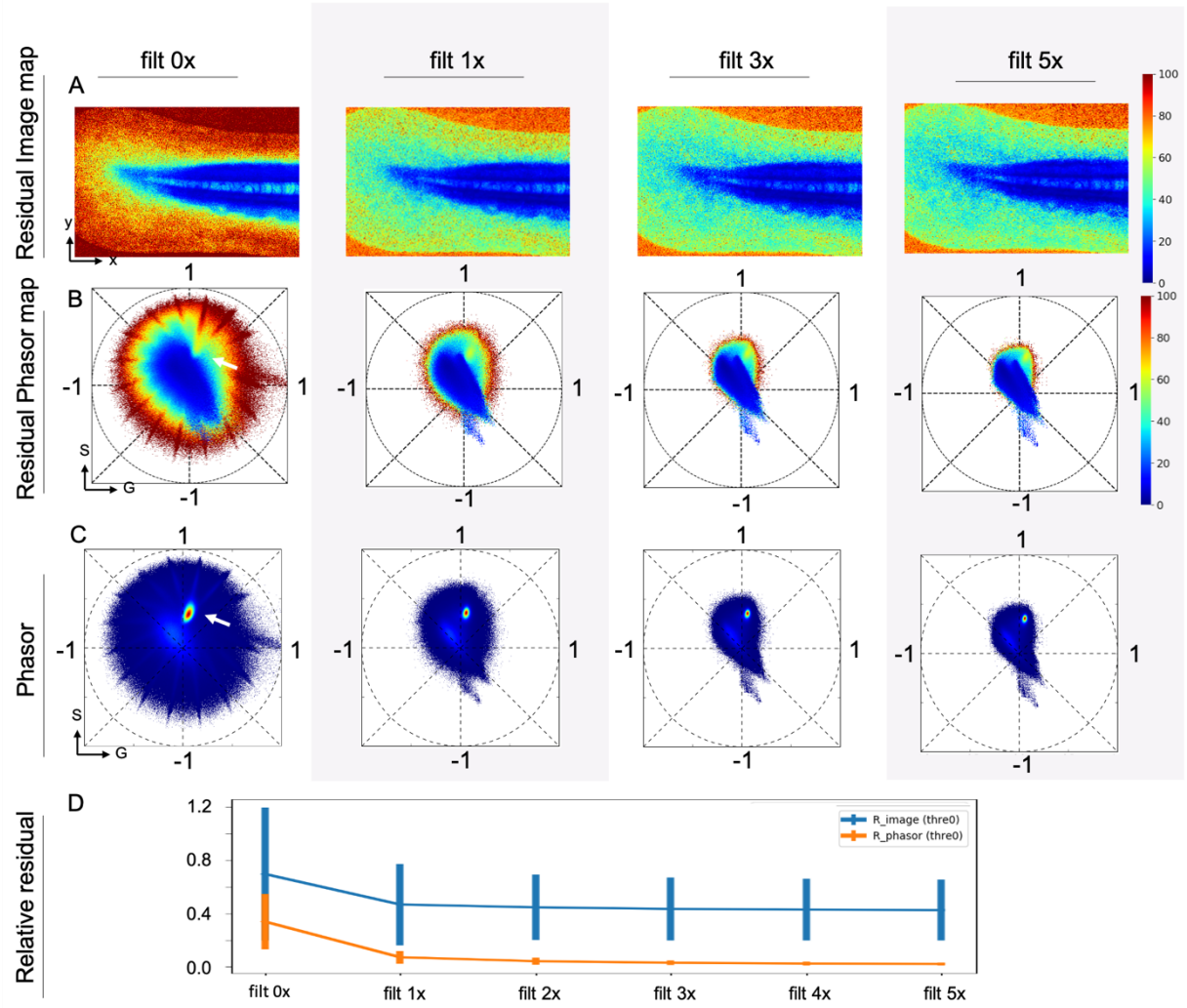

Supplementary Figure 9. Application of denoising filters reveals improved results with lower residuals. (A) Residual Image Map of HyU unmixing of a quadra-transgenic zebrafish Gt((cltca:);Tg(Citrine);(ubiq:); (ubiq:lyn-tdTomato); (-ubiq:Lifeact-mRuby);(fli1:mKO2)) inclusive of one strong autofluorescent signal. Residual values are calculated with different number of denoising filters[6]. The average relative residual visibly decreases with the increase of denoising filter numbers. **(B)** Residual Phasor Map shows a major decrease in values between 0 and 1 denoising filters, maintaining statistically similar values at higher denoising filter applications. **(C)** Phasor plots for different denoising filters. Phasor of raw data prior to denoising or thresholding, presents noise connected to each of the detectors, as well as a high count area corresponding to the background region. The phasor plot distribution highlights areas with higher pixel counts coming from the background noise, which correspond with lower Residual Phasor Map values in B. **(E)** Average residual values for Residual Image Map **(A)** and Residual Phasor Map **(B)** highlight that the improvement on residuals mostly focuses on the first

application of the denoising filter. In this initial denoising, the average relative residual decreased from 69.8% to 46.8%, further decreasing to 42.6% after 5 denoising. Average relative residual for phasor decreased from 33.9% to 7.1% after 1 denoising filter was applied, further decreasing to 2.1% after 5 denoising applied. With standard processing threshold of 250 digital levels applied (bottom 0.38% intensities of 16-bit format), the average relative residual decreased from 7.2% to 4.6%, further decreasing to 4.1% after 5 denoising filters. Average relative residual for phasor decreases from 10.1% to 2.6%, further decreasing to 1.1% after 5 denoising filters.

Supplementary Figure 10

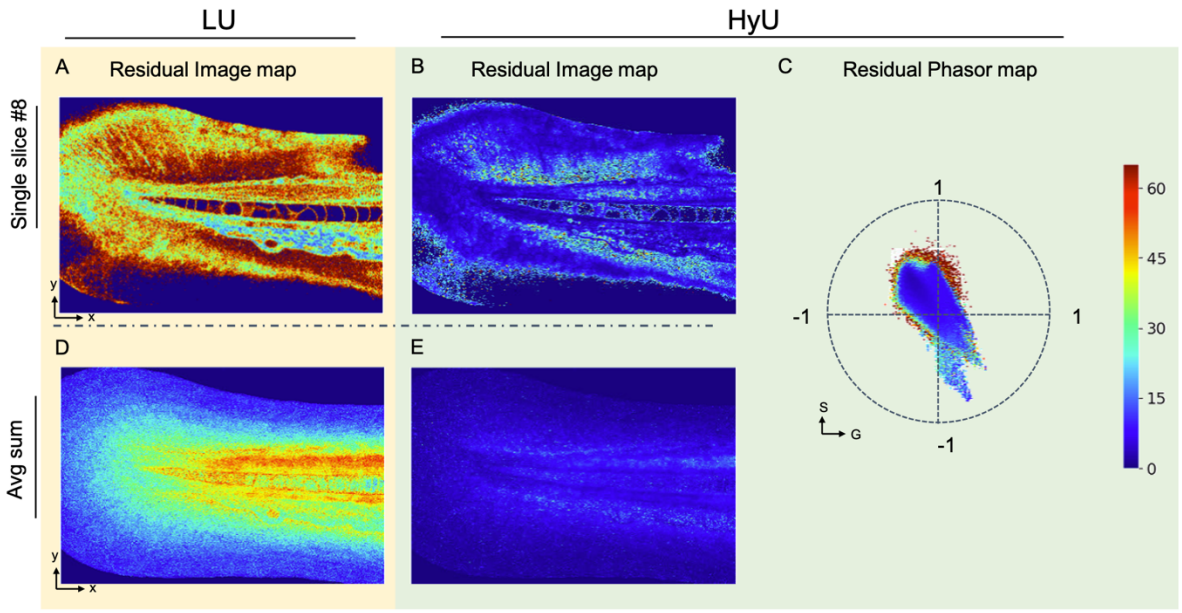

Supplementary Figure 10. Comparison of residual images for LU and HyU highlights improved HyU performance. Residual Image projection for LU and HyU of a 3D dataset of 3 dfp quadra-transgenic zebrafish GtTg(cltca-citrine);Tg(:Citrine);(ubiq:); (ubiq:lyn-tdTomato);(-ubiq:Lifeact-mRuby);(fli1:mKO2)) with an intensity threshold of 250. **(A)** LU Residual Image Map for a single slice (z=8 of 17 in a z-stack) provides average relative residual of 35.9%, while the **(B)** corresponding map for HyU averages at 7.1%. **(C)** Residual Phasor Map for the z-stack presents average relative residual of 1.1%. The reduction in residuals for HyU is maintained across the z-stack, as shown in **(D)** the average LU and **(E)** HyU Residual Image Maps built from the average of residuals across all z-slices. The average residual improvement for HyU at 4% compared to LU at 21% is 5.3-fold.

Supplementary Figure 11

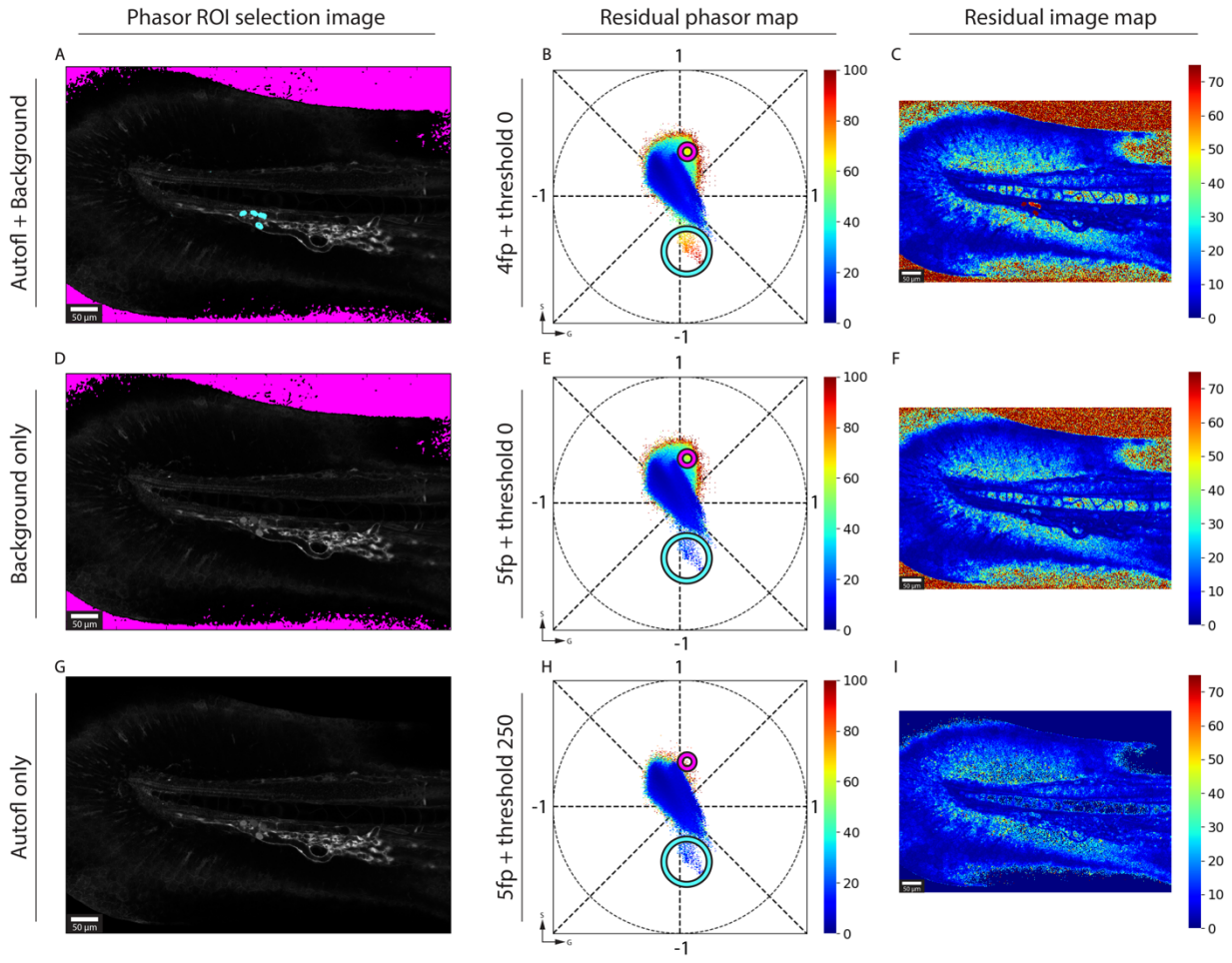

Supplementary Figure 11. Residual maps facilitate identification of independent spectral components. Experimental fluorescence microscopy data often includes unexpected autofluorescence signals. Residual Maps (Methods) provide additional information to account for these signals and properly adjust HyU analysis. **(A)** Average intensity image with pixels pseudo-colored in cyan (autofluorescence) and magenta (background) according to the ROIs selections on the **(B)** Residual Phasor Map, computed from the HyU of 4 input spectra with a threshold of zero. The pseudo-colored areas of the image match those presenting high residual values in the **(C)** Residual Image Map. Changing the unmixing input to include the unexpected autofluorescent spectrum (cyan) and performing the Residual Phasor map selections produces the **(D)** background pseudo-colored (magenta) image. The inclusion of autofluorescence as an independent spectral component in the unmixing decreases the number of pixels corresponding to the autofluorescent signal (cyan ROI) in the **(E)** Residual Phasor Map, thereby matching with the **(F)** Residual Image Map, which no longer presents high residuals in the center portion of the image. Increasing the threshold to 250 removes the pixels with high residuals corresponding to

the background, removing them from the **(G)** average intensity image, **(H)** Residual Phasor Map, and **(I)** Residual Image Map.

Supplementary Figure 12

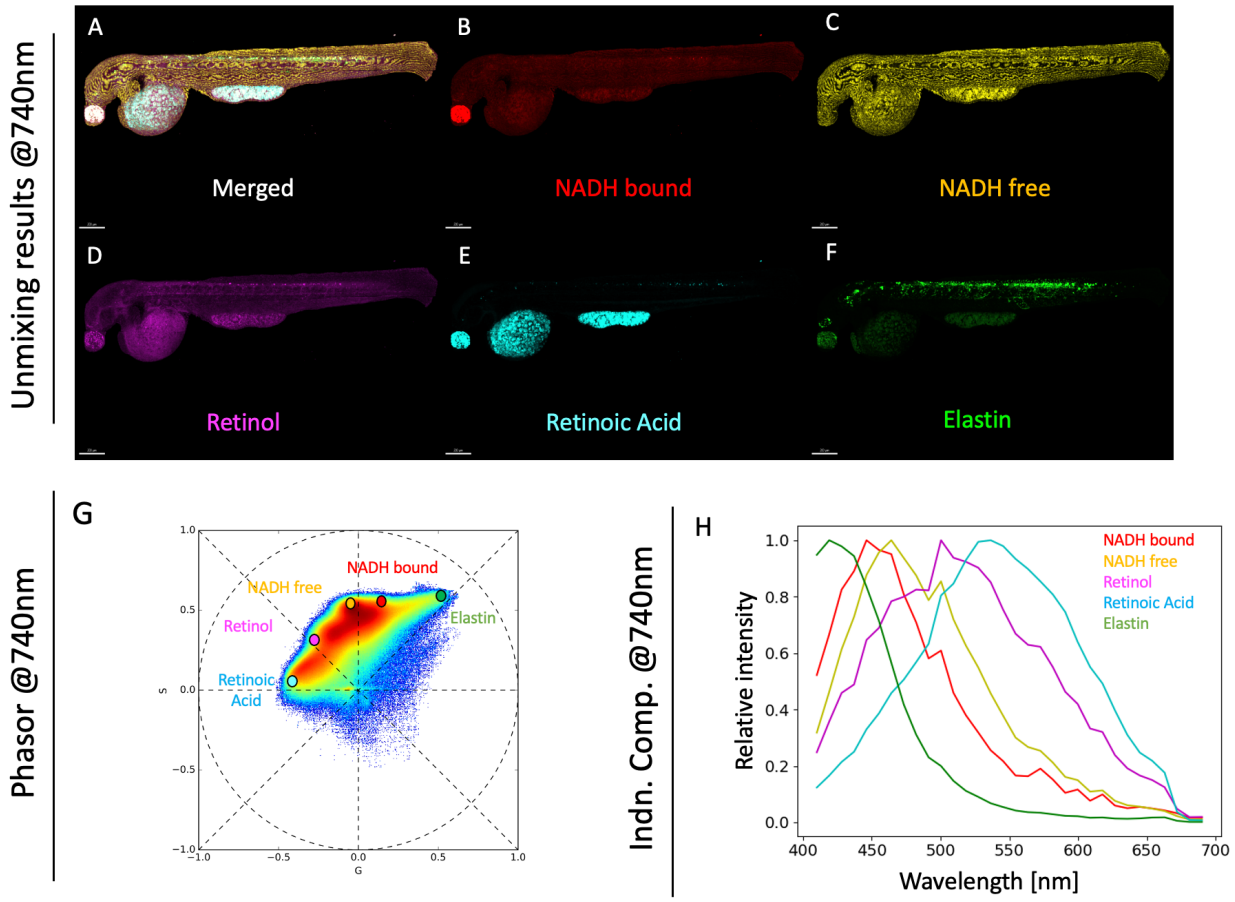

Supplementary Figure 12. HyU analysis of 36 hpf Casper zebrafish demonstrates feasibility of unmixing only intrinsic signals. Casper zebrafish is a transgenic zebrafish characterized by the absence of pigments. Dataset was acquired in the two-photon spectral mode @740 nm excitation. HyU Unmixing was performed utilizing 5 pure intrinsic signals measured in solution (Methods): **(A)** Merged overview of all signals **(B)** NADH bound **(C)** NADH free (yellow), **(D)** retinoid (magenta), **(E)** retinoic acid (cyan) which appears mainly in the yolk sac, known location where carotenoids are stored, transferred and then metabolized to retinoic acid [11] **(F)** elastin (green) has a similar distribution with in the zebrafish floorplate at this developmental stage **(G)** Phasor **(H)** average spectra from selection in **G**.

Supplementary Figure 13:

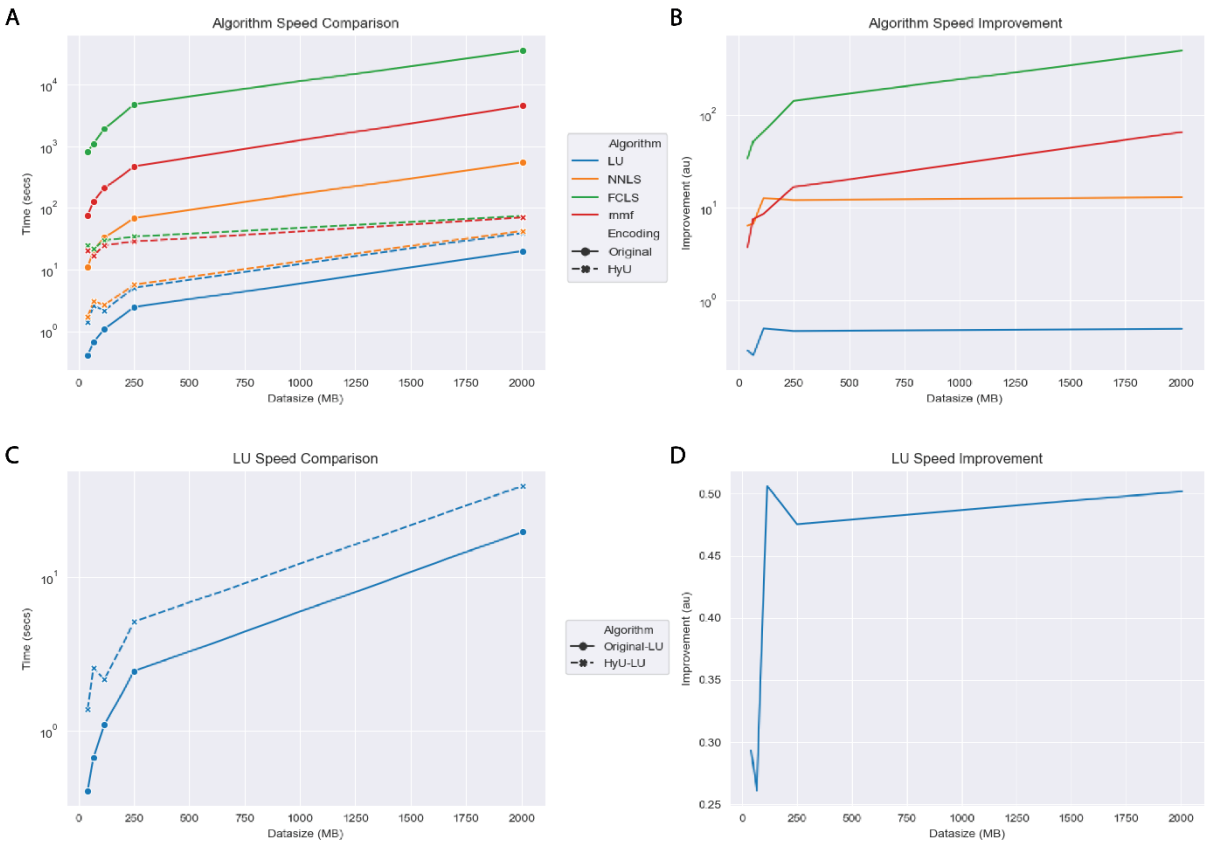

Supplementary Figure 13. Speed comparison and improvement plots of multiple unmixing algorithms in their Original form vs HyU encoded. **(A)** Computational times of multiple unmixing algorithms for both original (pixel-by-pixel) and HyU versions over a range of hyperspectral imaging datasets sizes. **(B)** Improvement in speed using the ratio of the HyU over the Original unmixings demonstrate a vast increase in speed for all algorithms other than LU across all input data sizes. **(C, D)** Computational times and speed improvement for original and HyU versions of LU show that the original version of LU provides higher computational speeds at ~2x. Plots **A-C** use logarithmic scales while plot **D** uses a linear scale for the y-axis.

Supplementary Figure 14

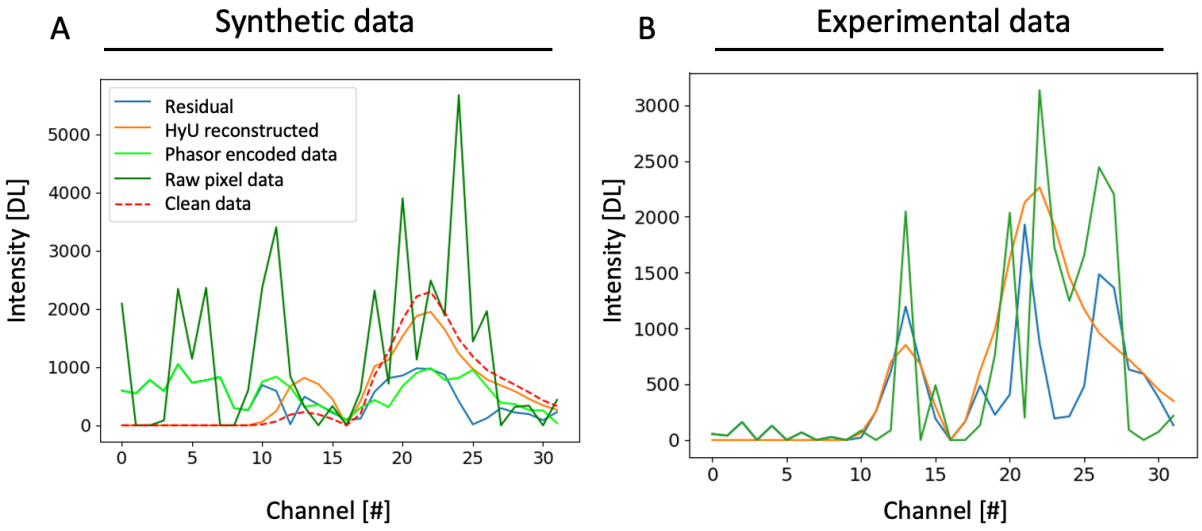

Supplementary Figure 14. Residuals in synthetic data and experimental data. **(A)** We simulated data with the purpose to cover wide ranges of noise and to allow for thorough testing of the algorithm's performance. In this example a ground truth spectrum with 14 photons (red dashed line) is simulated accounting for multiple types of noise (dark green line). The simulated spectrum presents disrupted shape with substantial presence of noise. During HyU analysis, in the encoding of spectra within a phasor bin, the simulated spectrum (dark green line) is averaged with similar spectra of multiple other pixels, producing (light green light). The spectrum recovered with Hybrid Unmixing (orange line) is similar to the ground truth. In the calculation of residuals, however, due to the disrupted signal of simulation (dark green line), the absence of noise in the clean data is counted as residual. **(B)** Spectrum from experimental data (from Figure 3) at a similar photon-range (15 to 20 photons) for comparison. The same color code is utilized for the spectra lines, without ground truth owing to the nature of experimental data.

Table S1 :

	Label	Zebrafish Stage	Imaged volume [pixels]	Imaged volume [pixels]	Imaged volume [pixels]	Lateral pixel (x,y,res.) [µm]	Axial section (z res.) [µm]	Pixel dwell time [µs]	Laser Power
Fig 2E-P, S7, Mov1	Gt(cltca-Citrine); Tg(ubiq:lyn-tdTomato; ubiq:Lifeact-mRuby; fli1:mKO2)	10 dpf	1024	1024	17	0.346	3.00	3.1	561 nm: 0.18% 488nm: 5%
Fig 3A-F, S1, S8	Gt(cltca-Citrine); Tg(ubiq:lyn-tdTomato; ubiq:Lifeact-mRuby; fli1:mKO2)	2 dpf	1024	512	31	0.415	5.00	3.1	561 nm: 0.6% 488 nm: 5.5%
Fig 4, Mov2	Gt(cltca-Citrine); Tg(kdrl:mCherry; fli1:mKO2)	5 dpf	512	1024	26	0.461	3.00	2.5	561 nm: 2% 488nm: 4%
Fig 5 A, S2	Gt(cltca-Citrine); Tg(ubiq:lyn-tdTomato; ubiq:Lifeact-mRuby)	3 dpf	2304	512	27	1.38	5.00	5.0	561 nm: 0.4% 488 nm: 2.8%
Fig 5 B-D	Gt(cltca-Citrine); Tg(ubiq:lyn-tdTomato; ubiq:Lifeact-mRuby; fli1:mKO2) Plus strong autofl	3 dpf	2560	2048	27	0.259	4.00	3.1	561 nm: 0.18% 488 nm: 5%
Fig5 E-G									740 nm: 4%
Fig 6, S9, S10,	Gt(cltca-Citrine); Tg(ubiq:lyn-tdTomato; ubiq:Lifeact-mRuby;	3 dpf	768	512	17	0.923	4.00	6.3	561 nm: 0.4% 488 nm: 5%

S11, Mov3	fli1:mKO2) Plus strong autofl								
S12	casper	36 hpf	6144	1536	25	0.461	6.00	3.1	740 nm: 3%

*hpf = hours post fertilization
*dpf = days post fertilization

Supplementary Note 1: Identification of spectra and new components with HyU

Identification of independent spectral components has been an adversity for unmixing hyperspectral data. First, the collected spectra may be distorted by reduced SNR. Secondly, excitation of intrinsic signals causes uncertainty of biological sample. Favorably, HyU simplifies this process by adapting Phasor approach and achieving semi- or full- automation process for spectra identification and selection. In HyU spectra can be loaded from an existing library, virtually automating the analysis process. Pre-identified cursors are generated from common fluorophores such as mKO2, tdTomato, mRuby, Citrine. In the presence of unexpected fluorescent signals, spectra can also be selected and visualized directly from the phasor. The "tails" on the phasor distributions are independent components. In our HyU graphical interface, clicking on the phasor visualizes the spectra within a small area (9x9 bins) of the phasor histogram (Figure 1 D). In the example in Sup. Figure 9-11 we identify 5 distinct endmembers on the Phasor (Sup. Figure 10, C), visualize their spectra identifying NADH bound, NADH free, Retinoid, Retinoic Acid and elastin. The use of Residual Phasor Map (Sup. Figure 11, B) allows for identification of areas in the phasor with high amount of residuals, likely corresponding to a missing endmember in the unmixing. Residual Image Maps (Sup. Figure 11, C) provide a rapid overview of residuals in the image data, for identification of location in the dataset of the missing endmember.

Supplementary Note 2: HyU in autofluorescent data

Cellular metabolism is a key regulator of cell function and plays an essential role in the development of numerous diseases. Understanding of cellular metabolic pathways is critical for the development and assessment of novel therapies and diagnostics. However, metabolic pathways are complex and changes are highly dynamic: changes can occur in the order of seconds or minutes or occur over a period of days, weeks, months and years and those metabolic changes are highly heterogeneous. A number of metabolites have been reported in literature to be fluorescent and to change their spectra according to their biochemical configurations. For example, the measurement of NADH in its free and bound state is possible thanks to a shift in the emission spectra when NADH is bound to enzymes such as Lactate Dehydrogenase (LDH). Likewise, retinol and retinoic are known to have different autofluorescent spectra. HyU is well posed for the analysis of intrinsically low autofluorescence owing to its ability to operate at low SNR. In Sup. Figures 12 we visualize unmixing of multiple autofluorescent signals based on spectra acquired from in vitro solutions.

Supplementary Note 3: Reduced computational costs during unmixing

An advantage of HyU is speed. HyU provides substantial speed boosts when comparing to other pixel-based unmixing algorithms. The exception is for standard LU vs HyU owing to the highly optimized computational implementation of the functions which are utilized in standard LU. This speed boost occurs because unmixing is performed at a phasor-histogram level, where a single bin corresponds to a multitude of image pixels. For algorithms other than standard LU, HyU provides up to ~500-fold improvement in speed at comparable coding language and computing hardware, processing 2 GB in less than 100 seconds (Supplementary Figure 13).

This improvement provides a solution for open image-analysis challenges in multiplexing fluorescence. First, the increased size of HFI data, resulting from continuously higher throughput and resolution microscopes, scaled with the number of spectral channels. Second, the number of datasets, owing to experimental reproducibility and biological variability.